ELSEVIER

Contents lists available at ScienceDirect

## Computers and Geotechnics

journal homepage: www.elsevier.com/locate/compgeo





# Evaluating Transient Drawdown and Slope Stabilization from Horizontal Drain Installation

Mahrooz Abed, Bipin Peethambaran, Ben Leshchinsky

Department of Forest Resources, Engineering and Management, 201 Peavy Forest Science Center, Oregon State University, Corvallis, OR 97331, United States

#### ARTICLE INFO

Keywords: Landslides Horizontal drains Landslide mitigation Dewatering Slope stability

#### ABSTRACT

Elevated groundwater levels drive slope instability through decreased effective stresses and frictional strength. Consequently, landslide mitigation often relies on a variety of stabilizing techniques, often including dewatering and drainage as a primary control on stability. One of the most effective dewatering techniques for landslides are horizontal drain systems, which consist of arrays of perforated pipes drilled into hillslopes for gravity-driven removal of groundwater. One of the few economical solutions for large-magnitude, groundwater-driven landslides, horizontal drain arrays facilitate groundwater drawdown through gravity-driven flow, consequently increasing effective stress and slope stability within its domain of influence. However, design of horizontal drain systems remain largely observational and there is limited insight towards the transient performance of these drainage systems. This study aims to explore relevant theoretical design criteria for horizontal drain systems and their relative importance as related to drawdown mechanism and magnitude, as well as slope stability.

## 1. Introduction

Horizontal drain systems are one of the few means of stabilizing large, active landslides driven by groundwater (Sedghi et al. 2009). These systems, commonly used throughout the world, are an inherently three-dimensional application, and its transient behavior is largely a function of drain array geometry, layout, site conditions, etc. Consequently, modeling that captures the three-dimensional drawdown behavior of horizontal drain (HD) systems over time is of practical relevance. Various studies have evaluated the three-dimensional and/or transient drawdown behavior of horizontal drain systems numerically or semi-analytically. Zhan and Zlotnik (2002) proposed a semi-analytical solution for three-dimensional transient flow to a horizontal or slanted well in an unconfined aquifer, however, this proposed solution was specific to a predefined pumping rate and not applicable to gravitydriven flow to HDs within hillslopes. Considering a fully penetrating stream parallel to a pumping horizontal drain, Huang et al. (2011) proposed an analytical solution developed through application of Fourier transforms to examine the effect of specific yield, drain depth and anisotropic hydraulic conductivity on a given spatial head distribution. Although these analyses demonstrated agreement with the analytical results of Zhan and Zlotnik (2002) and field experiment results of Mohamed and Rushton (2006), the proposed solution was suitable for a set of boundary conditions that are not fully applicable to landslide mitigation, where gravity-driven flow and recharge boundary conditions are of relevance.

Much of the rather limited research on subsurface drains and particularly HD systems were in agricultural applications (Dierickx 1999; Kirkham 1950; Stuyt and Dierickx 2006)), remediation of contaminated groundwater (Sawyer and Lieuallen-Dulama (1998)), municipal solid waste leachate flow control (Hu et al., 2021; Hu et al., 2020) and oil and gas exploration and extraction (Daviau et al., 1988; Goode and Thambynayagam, 1987; Joshi 1987). With advancement of drilling techniques, horizontal drains have been used widely for landslide mitigation purposes, however, a robust design considering major system elements of HDs including location, length, spacing and inclination angle of the pipes (Lakruwan et al., 2021) is largely observational, particularly under transient, three-dimensional conditions. For example, Lakruwan et al. (2021) performed laboratory experiments to understand horizontal drain discharge and drawdown geometry. Cai et al. (1998) modeled horizontal drains and slope stability under threedimensional conditions for a series of simplified, instructive examples. However, besides this work, most analyses consider the importance of horizontal drains considering valuable case studies, often under two-

E-mail addresses: abedma@oregonstate.edu (M. Abed), bipin.peethambaran@oregonstate.edu (B. Peethambaran), ben.leshchinsky@oregonstate.edu (B. Leshchinsky).

 $<sup>^{\</sup>ast}$  Corresponding author.

dimensional conditions (e.g. Tang et al., 2011; Sari et al., 2023; Taha (2011)) and limited exploration of the mechanisms of drawdown are considered.

As rainfall is one of the major causes of landslides, the efficiency of HDs in controlling groundwater rise due to rainfall was explored in numerous studies (Rahardjo et al., 2003; Rahardjo et al., 2011). Using a two-dimensional finite element model, Rahardjo et al. (2003) showed the effectiveness of HDs installed at three different depths and concluded that drains located at the lower part of the slope have the largest effect on drawdown of the aquifer. Similar findings were proposed by Zhang et al. (2023). Further, they found that for most practical applications in deep-seated landslides, consideration of unsaturated conditions is largely unnecessary (Rahardjo et al., 2003). Cai et al. (1998) studied the effect of length, spacing and direction angle of HDs to stabilize slopes using a three-dimensional finite element analysis of transient water flow for a limited set of slope geometries. Drain length was demonstrated to be a more effective control on drawdown than spacing between (i.e. increasing the number of drains) for the limited set of conditions considered. Using the equation proposed by Hooghoudt (1940) for steady-state groundwater height between horizontal drains on level ground, Crenshaw and Santi (2004) further developed a twodimensional approximation for drawdown from drain emplacement as related to wick drains, finding that there are optimal design conditions (e.g. spacing associated with specific soil textures and hydraulic

While much of the prior work focusing on horizontal drain systems is important, there is a lack of insight towards the three-dimensional transient conditions associated with drawdown from these systems. Further, the mechanisms by which this drawdown occurs and the magnitude of both discharge and enhanced slope stability are poorlyconstrained. This study focuses on development of a three-dimensional finite difference model capable of systematically describing both the mechanism and magnitude of transient groundwater drawdown as well as the stabilizing effects of horizontal drain systems. The importance of drain spacing, length, slope inclination, and other domain considerations are evaluated in context of drawdown and change in stability. The results are described for hillslope conditions outside of what has been considered in prior studies and are presented in dimensionless form for generalization. While select examples are presented, the proposed solutions provide a level of intuition as to the efficacy of these landslide mitigation systems.

#### 2. Methodology

#### 2.1. Steady-state flow

Prior to drain installation and drawdown, initial conditions of steady state flow in a homogenous saturated porous media with constant aquifer thickness  $(L_z)$  with slope angle  $(\beta)$  are considered. Considering a fixed head boundary condition representative of saturation at the toe of slope and a steady recharge at the upper boundary, the three-dimensional steady state groundwater flow is derived through coupling Darcy's law and the continuity equation

$$K_x \frac{\partial^2 h}{\partial x^2} + K_y \frac{\partial^2 h}{\partial y^2} + K_z \frac{\partial^2 h}{\partial z^2} = 0$$
 (1)

where h is total hydraulic head and is  $h=h_p+h_e$ , where  $h_p$  and  $h_e$  are pressure and elevation head, respectively;  $K_x$ ,  $K_y$  and  $K_z$  are hydraulic conductivity of the soil in  $x_xy$  and z directions, respectively. As flow velocities are rather small in soil and rock, velocity head is considered negligible and consequently ignored. Assuming a recharge boundary condition at the top of the slope, the constant recharge rate to keep the steady flow condition is calculated as:

$$Q_{\text{Re}} = \sqrt{\left(K_z \sin\beta\right)^2 + \left(K_y \cos\beta\right)^2} \frac{\partial h(x, L_y, z, t)}{\partial y'}$$
 (2)

where  $Q_{\rm Re}$  is recharge rate; and  $\partial y^{'}$  is the corrected form of  $\partial y$  which is defined as:

$$\partial y' = \sqrt{(\partial y \tan \beta)^2 + \partial y^2} \tag{3}$$

During the next model phase – drain installation - the recharge flux and steady state groundwater head obtained at this preliminary step is thereafter used as the boundary and initial conditions at the upper boundary, respectively.

#### 2.2. Flow to horizontal drain systems

After steady-state, slope-parallel flow conditions are attained from the aforementioned initial phase, a single gravity horizontal drain with length  $L_p$  is located at the center of the xy plane (Fig. 1). In order to capture groundwater drawdown, a three-dimensional nonlinear transient groundwater flow equation of an anisotropic medium is adopted:

$$S_{s}\frac{\partial h}{\partial t} = K_{s}\frac{\partial^{2}h}{\partial x^{2}} + K_{y}\frac{\partial^{2}h}{\partial y^{2}} + K_{z}\frac{\partial^{2}h}{\partial z^{2}} + Q \tag{4}$$

where the initial conditions are obtained from steady state conditions prior to drain installation are:

$$h(x, y, z, 0) = h_0 (5)$$

no-flow impermeable boundary conditions at the base are defined as:

$$\partial h(x, y, 0, t)/\partial z = 0 \tag{6}$$

instantaneous drainage boundary conditions are assigned at the top of the water table as:

$$K_z \partial h(x, y, L_z, t) / \partial z + S_y \partial h(x, y, L_z, t) / \partial t = 0$$
(7)

and the boundary conditions at the toe of slope with fixed head are:

$$h(x,0,z,t) = h_d \tag{8}$$

and the recharge boundary condition at the top of the slope is defined through prior calculation of recharge that yields steady-state conditions:

$$\partial h(x, L_{y}, z, t) / \partial t = Q_{Re} - \sqrt{(K_{z} \sin \beta)^{2} + (K_{y} \cos \beta)^{2}} \frac{\partial h(x, L_{y}, z, t)}{\partial y'}$$
(9)

where t is time;  $h_0$  is initial head; Q is pumping rate (considered to be zero in this study as gravity-driven drainage is considered).  $L_x$ ,  $L_y$  and  $L_z$  as shown in Fig. 1 are dimensions of the domain in x,y and z directions, respectively;  $S_s$  is specific storage;  $S_y$  is specific yield;  $z_{drain}$  is vertical distance of the drain from the bottom boundary;  $Q_{\rm Re}$  is the recharge rate obtained from previous step. Groundwater flows towards the drain through a hydraulic gradient, where pressure head in the pipe is assumed to be negligible. Therefore, a boundary condition of fixed elevation head based on location of the drain is chosen to represent the drain in systems:

$$h(x_{ed}, ye_d, z_{ed}, t) = h_{ed}$$
 (10)

where  $x_{ed}$ ,  $y_{ed}$  and  $z_{ed}$  represent spatial location of perforations on the drain with respect to the origin; and  $h_{ed}$  is elevation head at any point along the drain. It should be noted that in this study for simplicity the head loss due to entrance resistance of perforations is neglected. As the drain systems are typically installed in parallel arrays, the two lateral boundaries that are parallel to the drain are considered symmetrical. Hence, the boundaries on the side represent drawdown owing to the modeled drain and a series of drains located at  $L_x$  on center on both sides

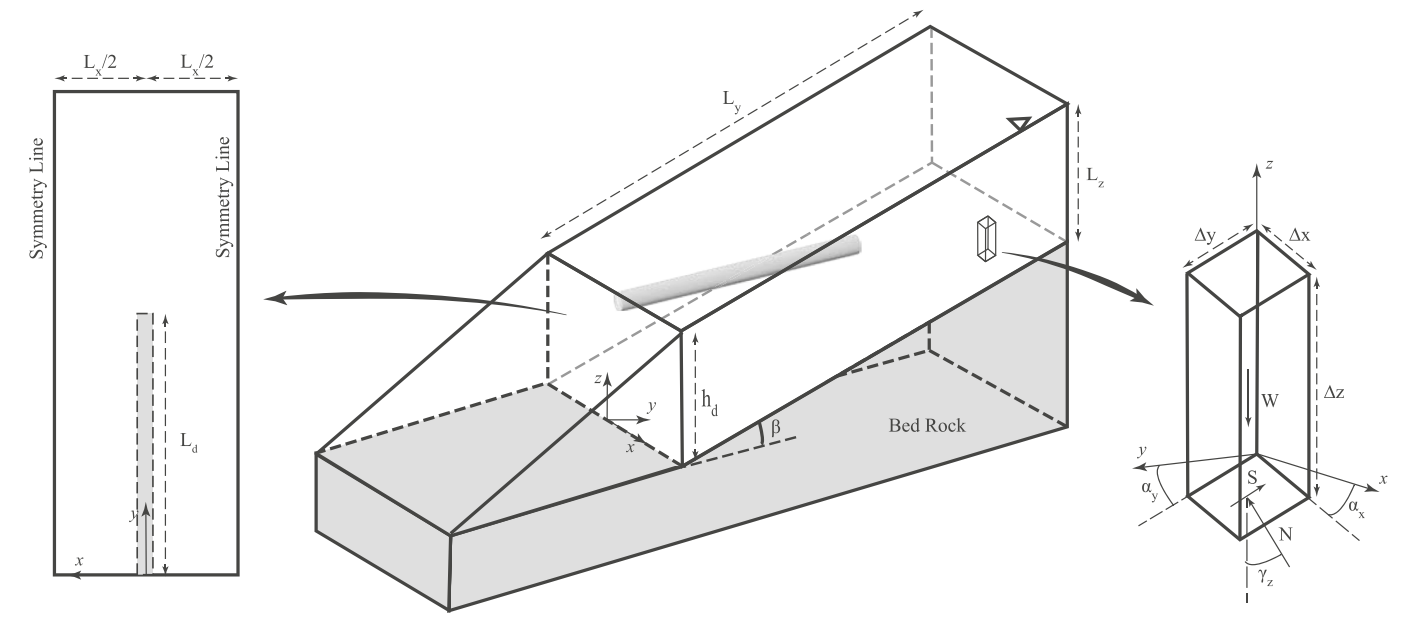


Fig. 1. Schematic diagram of aquifer, slope geometry, horizontal drain system and forces acting on each column of slope domain.

of the modeled drain.

#### 2.3. Horizontal Drain Discharge

The inflow rate along any point of the drain based may be approximated as:

$$Q_{in} = \sqrt{(K_x i_x)^2 + (K_y i_y)^2 + (K_z i_z)^2} A$$
(11)

where A is the surface area of a unit cylinder surrounding a drain; and  $i_x$ ,  $i_y$ , and  $i_z$  are hydraulic gradients in x,y and z directions, respectively, as follows:

$$i_{x} = \frac{\partial h(x_{d}, y_{d}, z_{d}, t)}{\partial x}$$
 (12)

$$i_{y} = \frac{\partial h(x_{d}, y_{d}, z_{d}, t)}{\partial y}$$
(13)

$$i_z = \frac{\partial h(x_d, y_d, z_d, t)}{\partial z} \tag{14}$$

Total flow within the drain can be obtained through summation of the discharge from each perforation from the end of the drain to its outflow point.

## 2.4. Slope stability

As drawdown from horizontal drains can arrest landslide movements through increased effective friction and consequently, enhanced stability, we investigate the effect of drain conditions through simplified, three-dimensional limit equilibrium analyses of slope stability. Drawdown from horizontal drains can be localized, where lowered head tends to occur along a "trench of depression" in proximity and above the drain system. However, drawdown tends to be more diffuse with increasing distance from a the drain system. These variable dradown conditions suggest that the stabilizing effects of horizontal drains have nontrivial three-dimensional effects; consequently a three-dimensional slope stability analysis is used to evaluate transient stability in response to dewatering. As horizontal drains are often installed in slopes that have exhibited signs of failure (e.g. creep, localized movement), the Factor of Safety is often near unity and the sliding surface is considered to be the

base of the aquifer (i.e. a depth of  $L_z$ ). As fully formed landslides tend to lack real cohesion, we ignore cohesion under these conditions. Under this working assumption, the mobilized friction angle (i.e. the friction angle that yields equilibrium) can be evaluated for each timestep. As drawdown occurs, the mobilized friction angle should decrease as effective stress and consequently friction increases. The change in stability is evaluated through time series of mobilized friction angles starting at drain installation and ending at steady-state conditions. Knowing elevation head at all locations for each step, pore water pressures can be directly evaluated and incoporated into slope stability analyses for a suite of hillslope domains. Hungr et al. (1989) proposed a three-dimensional horizontal force equilibrium analysis in the direction of sliding ( $\gamma$ ), defined as:

$$F = 1 = \frac{\sum (cA\cos\alpha_y + (N - u(t)A)\tan\phi\cos\alpha_y)}{\sum N\cos\gamma_z\tan\alpha_y + \sum kW + E}$$
 (15)

where F is a factor of safety set to unity; c is soil cohesion; A is true base area;  $\alpha_y$  inclination of sliding surface with respect to the direction of sliding; u is pore water pressure;  $\phi$  is friction angle;  $\gamma_z$  is the local dip of the sliding block; k is a horizontal earthquake coefficient; k is the total weight of the sliding block; k is the resultant of all horizontal components of applied point loads; and k is the normal force acting at the base of the block, derived from vertical force equilibrium as:

$$N = \frac{W - cA\sin\alpha_y - uA\tan\phi\sin\alpha_y}{m_\alpha}$$
 (16)

where  $m_a = \cos\gamma_z(1+\sin\alpha_y\tan\phi/\cos\gamma_z)$ . The mobilized friction angle,  $\phi_{mob}$ , is back-calculated for every time step for factor for the given pore pressure field to achieve a state of equilibrium. This is done through evaluating a suite of potential mobilized friction angles that satisfy the conditions of Equation (15). That is, when a mobilized friction angle yields equilibrium, the back-analyzed strength for that transient pore pressure field is determined and the change in mobilized friction versus initial conditions can be evaluated. A negative change in  $\phi_{mob}$ , denoted  $\Delta\phi_{mob}$ , reflects enhanced stability (i.e. less friction required for equilibrium). In this study, we present  $\Delta\phi_{mob}$  as a positive value for enhanced stability for clarity. In it's simplest form assuming a metastable landslide at initiation conditions (i.e. t=0, F=1),  $\Delta\phi_{mob}$  can be used to evaluate the true evolving factor of safety for each timestep as  $F(t)=\tan(\phi_{mob}(t=0))/\tan(\phi_{mob}(t=0)-\Delta\phi_{mob})$ ; however, we choose to

simply present the change in mobilized strength as it enables evaluation of factor of safety based on the friction angle at initial conditions. Future analyses could use more complex three-dimensional slope stability mechanisms than the simple basal sliding surface posed herein (e.g. Alberti et al., 2022), but these results still quantitatively demonstrate the role of horizontal drains as a stabilizing technique.

#### 2.5. Numerical solutions

Applying forward-stepping, central space method of discretization of finite difference approach to Eqs. (1) to (14), the partial differential equations of three-dimensional, transient groundwater change were solved numerically. A uniform spatial discretization was chosen for all dimensions to approximate the changes in total head at each time step. A sensitivity analysis was performed to ensure that model discretization was sufficient as to preclude solution sensitivity. Time steps were limited to a calculated minimum based on spatial discretization and soil properties to maintain stability (i.e. a Courant number). The fully coupled transient groundwater flow and mobilized friction angle finite difference solutions have been implemented in custom scripts in MATLAB, used for all of the analyses in this study. A steady state condition was considered met upon reaching a mean change tolerance of  $10^{-8}$  m of head for all nodes between each time step, which is calculated by root mean square deviation.

#### 2.6. Dimensionless conditions

For comparison purposes and generalization of presented solutions, we simplify model inputs and outputs by making them nondimensional. By providing dimensionless parameters, type curves can be derived to provide specific solutions. Considering d as the thickness of the aquifer, the dimensionless parameters are defined as:

$$L_xD = L_x/dL_yD = L_y/dL_zD = L_z/dh_D = h/dL_dD = L_d/d$$
 (17)

$$T_D = \frac{K}{S_c d^2} t \tag{18}$$

$$D_D = \frac{h_0 - h}{d} \tag{19}$$

$$Q_D = \frac{Q_{in}}{Kd^2} \tag{20}$$

$$K = (K_{\rm r}K_{\rm v}K_{\rm r})^{1/3} \tag{21}$$

where subscript "D" indicates dimensionless form of their corresponding counterparts introduced previously.

## 3. Model validation

The results obtained from the proposed numerical simulation are compared with analytical solutions of horizontal wells subject to pumping in an unconfined aquifer by Zhan and Zlotnik (2002), physical experimental of gravity-driven horizontal drains performed by Lakruwan et al. (2021) to evaluate model accuracy and groundwater drawdown by horizontal drains at Pioneer Mountain-Eddyville (PME) highway realignment (Cornforth Consultants Inc, 2013). The numerical solution is compared versus both approaches herein.

## 4. Comparison against semi-analytical solutions

Zhan and Zlotnik (2002) suggested a semi-analytical solution for three-dimensional transient groundwater flow in an anisotropic medium to evaluate pumping-induced drawdown near a horizontal well in an unconfined aquifer. A point source with pumping rate of Q was placed at  $(x_0,y_0,z_0)$  and was subject to initial conditions proposed in Eq. (5), no

flow conditions at the base of the aquifer as shown in Eq. (6), and instantaneous drainage boundary conditions at the water table as Eq. (7). Lateral boundaries at infinite distance from the horizontal well were considered with the following fixity:

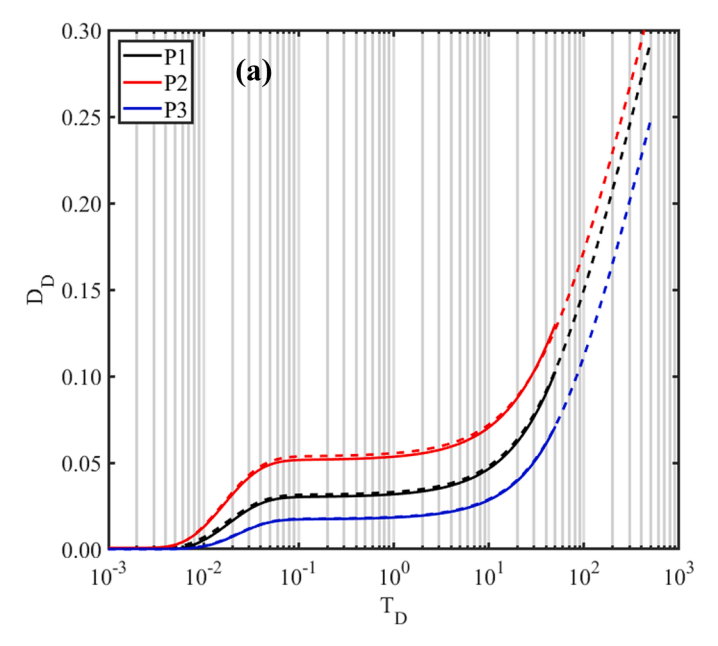
$$h(\pm \infty, y, z, t) = h(x, \pm \infty, z, t) = h_0$$
(22)

By applying a Laplace transform to Eq. (4) and the boundary and initial conditions of Eqs. (5), (6), (7) and (22), Zhan and Zlotnik (2002) solved the equations of transient groundwater flow into a semianalytical solution. To compare and validate the numerical solution proposed approach, the boundary and initial conditions were modified to represent the solution conditions of Zhan and Zlotnik (2002). Fig. 2a compares the results of dimensionless transient groundwater drawdown with fixed head lateral boundaries for a point sink located at the center of the unconfined aguifer based on semi-analytical method proposed by Zhan and Zlotnik (2002) and the numerical methods proposed in this study. Water drawdown in piezometers P1, P2 and P3 (locations shown in Fig. 2b) are compared. P1 and P3 are located at the same elevation as the source point and P2 is at the same location as P1 but at the base of the system. Comparing the drawdown of Zhan and Zlotnik (2002) semianalytical solution to proposed numerical method at the initial drawdown times shows underestimation for numerical solution (average of 20 %) for P1 and becomes less significant for P3 (average of 12 %) and P2 (average of 3 %). However, the difference between the solution of two methods begins to diminish as the drawdown continues to final stages and becomes more accurate within 1 % for P1 and P2 and 0.6 % for P3. The dimensionless drawdown in the three piezometers determined from the proposed numerical approach and the semi-analytical approach of Zhan and Zlotnik (2002) show reasonable agreement, especially for longer timescales relevant to the function of horizontal drain systems.

## 4.1. Comparison against physical models

An physical model of horizontal drain drawdown behavior was constructed and analyzed by Lakruwan et al. (2021) to monitor the effect of different perforation geometries on drawdown at steady-state conditions. The physical model consisted of a tank filled with sand and a single horizontal drain located at the bottom of the tank. Five strategically placed piezometers were used to measure pressure head during drain operation. An air pressure system was used to saturate the sand and maintain constant heads of 2 m, 1 m and 0.5 m (Lakruwan et al., 2021). A schematic of the aforementioned test setup is presented in Fig. 3a. Constant piezometric levels and subsequently constant discharge values (measured at the drain outlet) were indication of achieving steady state conditions. The experimental setup was modeled numerically to validate the applicability of the proposed approach. To achieve this, the boundary and initial conditions of the numerical method was modified to match the experimental test setup, which were constant head condition of 2 m and 1 m at the soil surface, and no flow boundary condition  $(\partial h/\partial x = 0)$  on all other sides of the tank.

Fig. 3b shows the steady state water head level corresponding to 1 m and 2 m constant head conditions obtained by proposed numerical method compared with corresponding experimental results. For both constant head condition, the formation of cone of depression was evident at the initial stages of drawdown. As the drawdown continued, head levels at the outer boundaries also decreased and eventually stabilized after reaching steady state conditions. The steady state conditions determined from the proposed numerical approach was defined as changes of head level was less than a tolerance of 10<sup>-8</sup> m between time steps. The experimental results of Lakruwan et al. (2021) and proposed numerical results shows agreeable results with slight overestimates or underestimates depending on the constant head conditions considered.



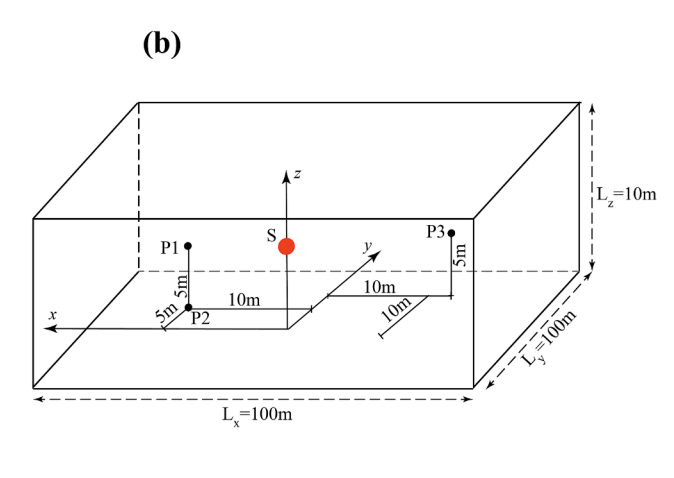


Fig. 2. (a) Comparison of semi-analytical solutions of transient dimensionless groundwater drawdown, DD, from Zhan and Zlotnik (2002) (dashed line) and numerical solution proposed in this study (solid line) (b) Schematic of the aquifer and sink point and location of piezometers at points P1(10 m,5m,5m), P2(10 m,5m,0m), and P3(10 m,10 m,5m).

#### 4.2. Comparison against field data from the oregon coast range

A realignment of US Highway 20 in Oregon initiated in 2005, where it was discovered the project is located on unstable Tyee Formation spanning and construction traversed series of paleolandslides (Hammond et al., 2009; Jones et al., 2023). As a mitigation plan, 170 km of horizontal drains were installed within the four paleolandslides. Mitigation of these landslides required extensive management of groundwater as well as mechanical stabilization, including rock buttresses, shear keys and anchors (Jones et al., 2023). Herein, we select one example of drawdown from a well-characterized piezometer determined from public documents. The horizontal drains placed at Pad C6H had an average length of 250 m and average inclination of 1.6 degrees - this drain system was chosen for comparison of the proposed numerical model against vibrating wire piezometer data recorded by piezometer C6-12 that was located in proximity of drain pad (Cornforth Consultants Inc. 2013 #126). The drains are located at depth of 30 m within the drain array, which had an average spacing of 2.8 m between the drains. Based on inferred site conditions ( $K = 1 \times 10^{-4}$  m/s for highly fractured rock,  $S_v = 0.2$ , Hammond et al., 2009, Jones et al., 2023), the boundary conditions of the numerical solution were assumed to maintain a constant head at upslope and downslope boundaries of upslope and downslope and no flow at sides and bottom and instantaneous drawdown at the top of the aquifer owing to the large domain and extensive recharge within the wet, cool rainforest of the Oregon Coast Range. Fig. 4 shows a comparison of real and modeled groundwater drawdown stemming from horizontal drain installation from the aforementioned piezometer, located at a depth of 28 m to the west of drain pad centerline (Cornforth Consultants Inc, 2013 #126). As shown, the model slightly overestimates drawdown, but largely captures the overall drawdown behavior. The discrepancies between the drawdown curves may owe to a variety of factors, including simplifying assumptions about the model (isotropic conditions, simplified geometry, variable drain patterns, etc.). In particular, the model considers drain installation as an immediate process as opposed to the real timing it takes to install a system, let alone a single drain. However, as a first order estimate on drawdown and its timing, the model provides reasonable estimates that could inform simplified design alongside conservative assumptions regarding margins of safety. Further, the drawdown behavior is nonlinear, and mimics the stages of drawdown observed from the proposed model, described in more detail later in this study. Further field verification would better isolate the role of some of these uncertainties and improve model performance.

## 5. Results and discussion

There are several design parameters that control the efficacy of HD systems as a means of reducing pore pressures and improving slope stability. Herein, we explore the sensitivity of dimensionless drawdown and stability to these parameters (drain length, drain spacing, inclination, domain size) for parallel HD arrays. As the evaluation was performed in dimensionless conditions, geometry and material properties such as hydraulic conductivity and specific storage were not directly considered as a variable in this analysis. Since the spacing and length of the drain are considered dominant parameters of HD design, we focus sensitivity analyses on these conditions and evaluate mean drawdown, mobilized friction angle on the sliding surface at the base of the aquifer and total outflow discharge. It should be noted that due to minimal sensitivity of the drain inclination on drawdown, in our analysis the drains are assumed to be installed with zero degree of inclination (i.e. horizontally). The geometry shown in Fig. 1 applies to all analyses presented and the landslide was assumed to be fully saturated initially  $(h_0 = d)$ , the drain was placed at the toe of landslide, i.e.  $h_d = L_z = d$ , and symmetric conditions were used to reflect drain spacing. The drawdown was calculated as the difference between initial head and the water head level obtained by proposed numerical model at each time step  $(D = h_0 - h)$ . As drawdown varied throughout the landslide volume, in the following discussions we simplify model time series by presenting mean drawdown over the entire sliding surface at the base of the aquifer.

## 5.1. Mechanisms of drawdown

Transient drawdown behavior may be highly nonlinear owing to the mechanism by which groundwater is removed from the landslide domain. We generally observe three different stages of drawdown that are sensitive to drain length, drain spacing, slope angle and length of the aquifer. Fig. 5 shows the three stages of transient groundwater drawdown before reaching steady state conditions for a drain array with

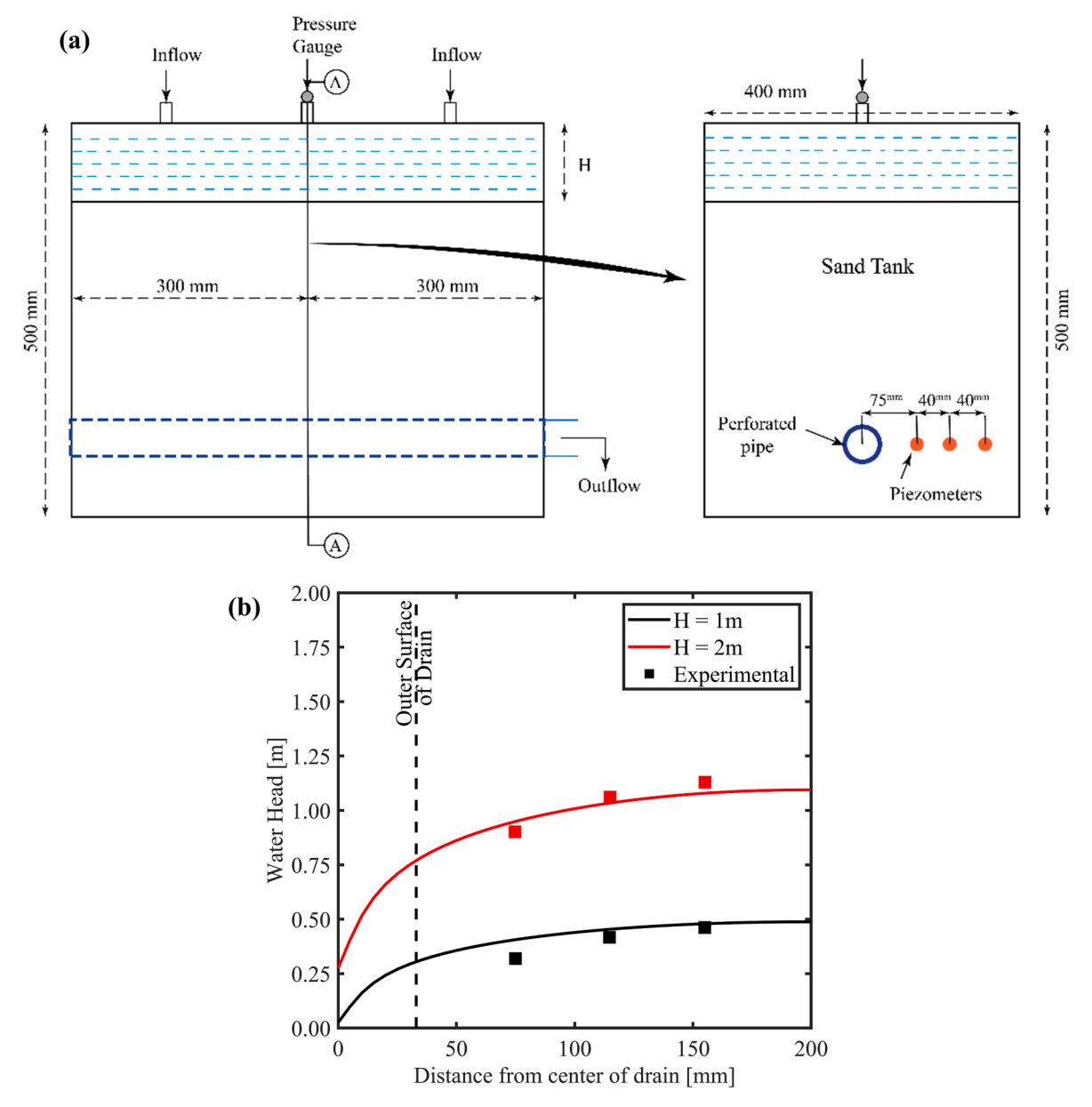


Fig. 3. (a) Schematic of experimental physical model of horizontal drain in sand tank and location of the piezometers (after (Lakruwan et al., 2021)) (b) Comparison of water head level of numerical modelling and physical model of Lakruwan et al. (2021) at the piezometers location.

conditions of  $L_{dD}=4$  and  $L_{xD}=1.6$  in an aquifer with  $\beta=~10~^\circ$  and  $L_{yD} = 5$ . The three stages of drawdown indicate an initial rapid drawdown, initiated with formation of a cone of depression, an intermediate stage with slower rate of drawdown and full development of cone depression, followed by a final rapid drawdown stage. Thereafter, steady state conditions persist. The first stage owes to drawdown immediately above the drain which happens rapidly due to proximity of standing water to the drain (Fig. 6a). Consequently, there is rapid formation of a cone of depression in the close proximity to the drain. In the second stage (Fig. 6b), the cone of depression grows both between parallel drains and upslope, influencing a larger aquifer area. The head contour curves in Fig. 6b and distribution of head along the drain implies the nonlinear groundwater drawdown behavior that stems from HDs. In the third stage (Fig. 6c), a final sustained drawdown phase occurs where the groundwater upslope of the drain system is drastically lowered in comparison to the previous stages and the drawdown continues until equilibrium between recharge and flow of water into the drain is achieved. The three stages (Fig. 5) show the general nonlinear

drawdown mechanisms of HD systems which are observed in some form regardless of the domain geometry or drain specifications. Variations of drain length and spacing and/or aquifer size can increase or decrease the duration of each of the stages and the volume of water being drawn into the system.

## 5.2. Influence of drain length

Drain length strongly controls drawdown and head conditions in an aquifer. Fig. 7a compares variation of average drawdown with drain length on the sliding surface at the base of the aquifer at the steady state for different slope angles ( $\beta=10^{\circ}$ ,  $20^{\circ}$ ,  $30^{\circ}$ , and  $40^{\circ}$ ) and aquifer length ( $L_{yD}=2.5$  and 5). The parallel spacing between the drains is set as  $L_{xD}=0.2$ . With the increase of normalized drain length from 0.25 to 2.5, the steady-state average drawdown increases from 0.008 to 0.20 for  $\beta=10^{\circ}$  and from 0.18 to 0.45 for  $\beta=20^{\circ}$ . For steeper slope angles ( $30^{\circ}$  and  $40^{\circ}$ ), extending the drain over a specific length does not create higher drawdown due to the influence of geometry and contact of drain tip into

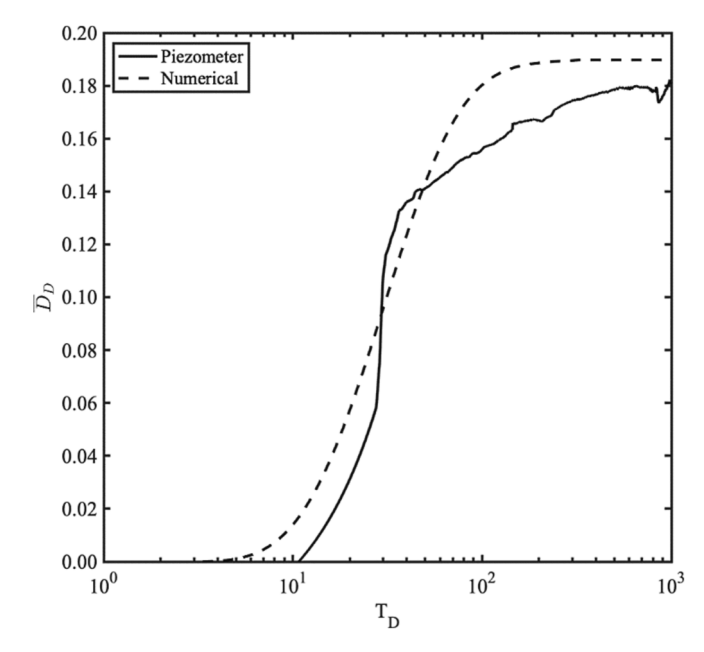


**Fig. 4.** Comparison of drawdown by numerical modelling and against field data for horizontal drains (Pad C6-H) located at US HWY20 (Cornforth Consultants Inc. 2013).

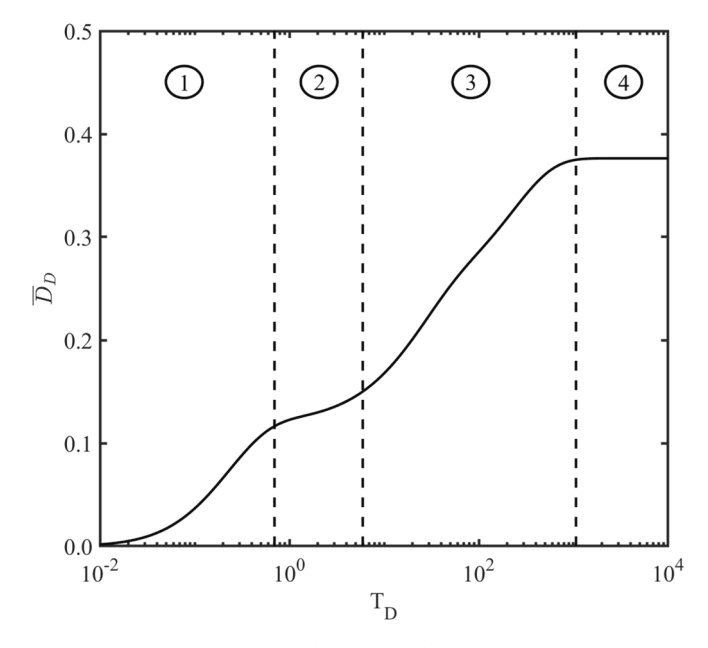


**Fig. 5.** Stages of transient groundwater drawdown for  $L_{dD}=4$ ,  $L_{xD}=1.6$ ,  $L_{yD}=5$  and ...  $\beta=10^{\circ}$ 

bedrock (assumed impermeable in these analyses) that limits the effective length of the drain. However, for a specific drain length shorter than the limiting length (e.g.  $L_{dD}=1$ ) installing drain in steeper slopes invokes higher drawdown at steady state conditions. This can be explained by the higher initial head above the drain elevation, driving a larger hydraulic gradient for gravity-based flow.

By lengthening the aquifer  $(L_{yD})$  from 2.5 to 5, the volume of water at the upper region of the drain increases and the drain influences a larger area. Shorter drains have a smaller area under their influence and the difference of the drawdown between  $L_{yD}=2.5$  and  $L_{yD}=5$  is not significant. By extending the drain length, larger area of the aquifer is impacted by the drain and the difference between the average drawdown for  $L_{yD}=2.5$  and  $L_{yD}=5$  becomes more notable. Steeper slopes

demonstrate significant differences between aquifer sizes when the drain length increases.

The head on the sliding surface at the base of the aquifer and the corresponding pore water pressures has a direct impact on slope stability and mobilized friction angle. Fig. 7b shows the variation of absolute change of mobilized friction angle on the sliding surface with drain length at the steady state condition for different slope angles and aquifer length regarding the average drawdown presented in Fig. 7a. With the increase of drain length, the mobilized friction angle increases significantly for any slope angle and a quifer length, that for  $L_{dD}=1$ , there is 1. 6° increase of mobilized friction for  $\beta = 10^{\circ}$  and 26° for  $\beta = 40^{\circ}$  for the aquifer length of  $L_{\nu D}=2.5$ . However, the impact of HDs is controlled by the geometry of the sliding block, that the changes of mobilized friction angle does not exceed certain values for each slope angle even by extending drain length. Installing the HDs in steeper slopes is more influential in larger aquifers as compared to smaller ones. As an example, for the drain length of 1.75 installed in  $\beta = 20^{\circ}$  enhances the mobilized friction angle  $10.5^{\circ}$  and  $12.3^{\circ}$  for  $L_{VD} = 2.5$  and  $L_{VD} = 5$ , respectively, and for drain in a landslide with and  $\beta = 30^{\circ}$  improves the mobilized friction angle to  $21.13^{\circ}$  and  $23.42^{\circ}$  for  $L_{vD}=2.5$  and  $L_{vD}=5$ , respectively. This comparison implies the faster rate of improvement of mobilized friction angle for steeper slopes with larger aquifers lengths.

The total outflow discharge is the result of the accumulation of the gravity driven water into the drain through circumferential perforations extended longitudinally on the drain. Fig. 7c shows the variation of total outflow discharge at steady state condition with drain length regarding different slope angles and aquifer length. The total discharge is dependent on the hydraulic gradient in proximity to the drain area, therefore, gravity driven drain system has equal steady state total outflow discharge regardless of the aquifer length indicating the significant dependence of discharge on drain length. By increasing drain length, the total discharge increases accordingly due to larger surface area for drawing groundwater, however, the rate of total discharge increment is higher for steeper slope angles, that for a drain with  $L_{dD} = 1$ , there is a 471 % increase in total outflow discharge, when slope angle increases from 10° to 40°. The increased efficacy of horizontal drain systems in lowering groundwater in steeper aquifers owes to larger hydraulic gradients along the drain length. That is, the drains are installed horizontally while the phreatic surface follows the contours of the hillslope – in such an scenario, there is an increasingly large head difference that scales with pipe length and embedment. These larger head differences yield (1) higher hydraulic gradients, (2) faster rates of drawdown and pore pressure decrease, (3) amplified rates of discharge, and (4) increased slope stabilization. Of course, the conditions posed herein are idealized, but do suggest that installation of horizontal drains within steeper hillslopes or at hillslope toes will yield improved drawdown and stabilization.

In order to show groundwater drawdown mechanisms before achieving steady state conditions, four distinct drain and landslide/ aquifer geometries are chosen to further highlight their transient behavior. Four scenarios are shown with points as Cases 1, 2, 3 and 4 in Fig. 8, where Case 1 is  $L_{dD} = 2$  and  $L_{yD} = 5$ , Case 2 is  $L_{dD} = 1$  and  $L_{yD} = 1$ 2.5, and both have similar slope angles of 20°. Case 3 and 4 have similar specifications as Case 1 and 2, respectively, but the drain is located in a  $10^{\circ}$  slope. The spacing between the drains for all cases are set to  $L_{xD} =$ 0.2. Fig. 8a shows the transient average groundwater drawdown on the sliding surface at the base of the aquifer for Cases 1 to 4. Case 1 distinctly shows all three stages of drawdown, with significant drawdown occurred during third stage that is related to larger upslope area feeding the aquifer. However, by decreasing the slope angle to 10° for the same drain and aquifer lengths (Case 3), the intermediate stage of drawdown diminishes and drawdown more smoothly increases to steady state conditions from first stage to third. Comparing Cases 3 and 4 with equal slope angles shows the controlling role of drain and aquifer length on drawdown mechanisms, reflected by relatively smooth transitions from

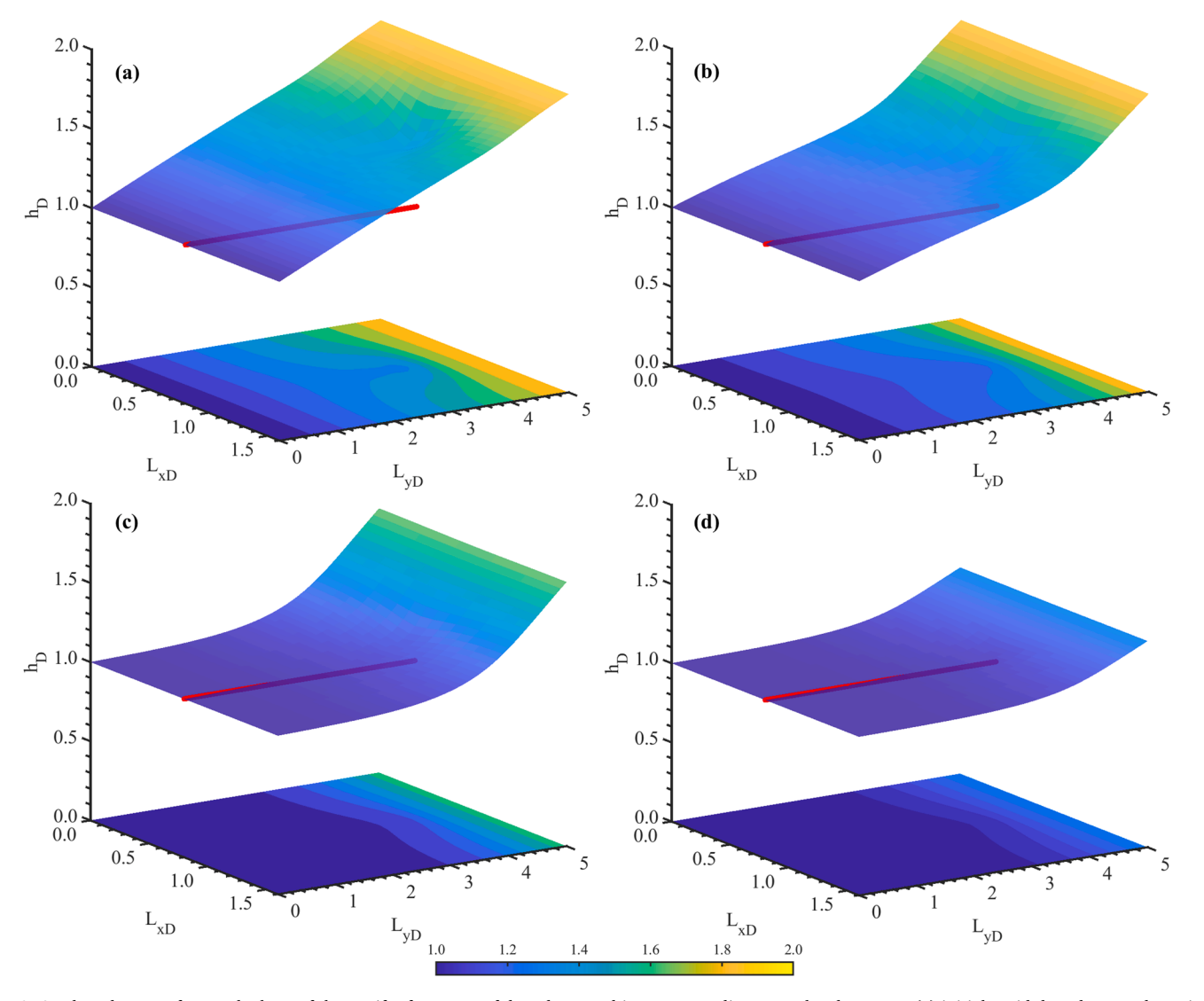


Fig. 6. 3D drawdown surface at the base of the aquifer for stages of drawdown and its corresponding water head contour: (a) initial rapid drawdown and starting formation of cone depression, (b) slow rate intermediate stage and fully formed cone of depression, (c) final rapid drawdown and lowering of upslope groundwater, (d) achievement of steady state conditions.

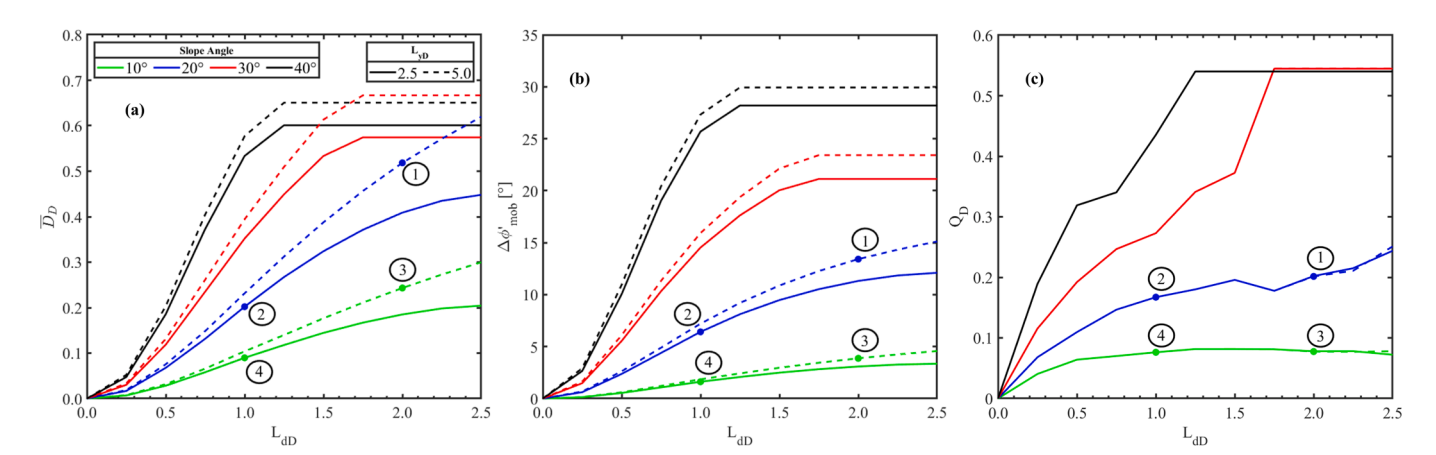


Fig. 7. Steady state (a) average drawdown, (b) mobilized friction angle at the slip surface corresponding to drawdown, (c) total outflow discharge of the drain vs drain length  $(L_{dD})$  for different slope angle  $(\beta)$  and aquifer length  $(L_{yD})$ .

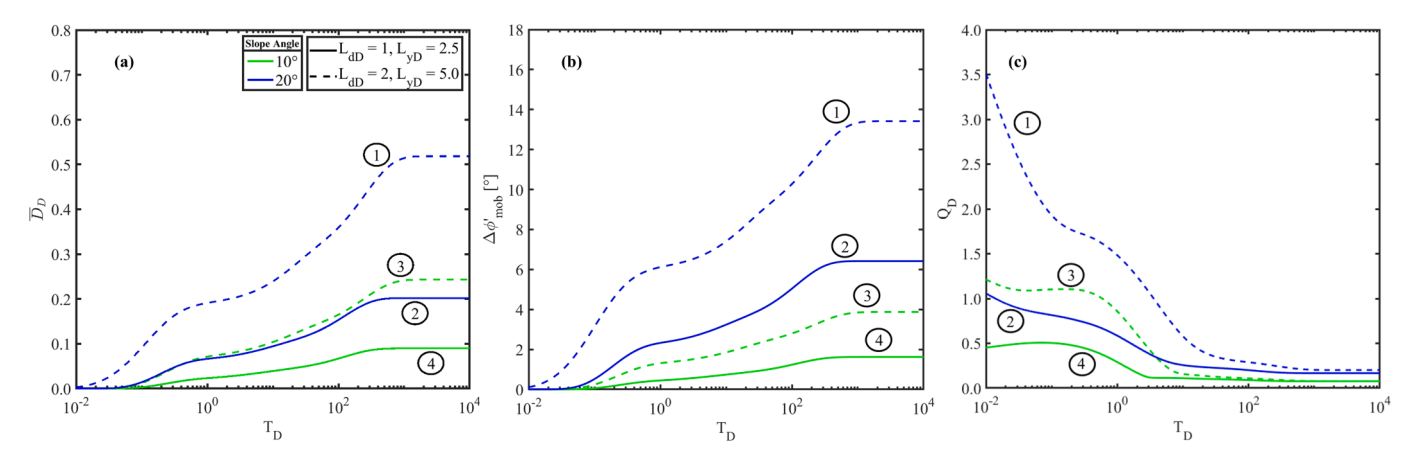


Fig. 8. (a) Transient average drawdown, (b) corresponding mobilized friction angle, (c) total outflow discharge for cases 1, 2, 3 and 4.

stage one to three (a minimal second stage) until achieving steady state conditions.

Fig. 8b shows transient absolute changes of mobilized friction angle on the sliding surface at the base of the aquifer corresponding to the drawdown shown in Fig. 8a. The most notable enhancement of mobilized friction angle occurred at slope angle of  $20^\circ$  where the largest changes in stability happened in the third stage, associated with drawdown of upslope boundary. As the slope angle decreases to  $10^\circ$ , the changes of mobilized friction angle upon installing HDs becomes smaller and the changes are smoother from initial stage to steady state conditions. Overall, longer drains are significantly more effective in improving stability, even if the aquifer is large (comparing Cases 1 and 2 and Cases 3 and 4).

The transient total outflow discharge for Cases 1 to 4 is shown in Fig. 8c, indicating initial higher discharge rates for larger aquifers (Cases 1 and 3). However, by continuing drawdown until achieving steady state conditions, all scenarios show similar outflow discharge rates, indicating considerable effects of drain length on initial stages of flow, and a less influence at steady state conditions, where hydraulic gradient near the drain systems become similar.

## 5.3. Influence of drain spacing

The spacing between drains is frequently considered one of the most important parameters controlling the efficacy of HD arrays (Crenshaw and Santi, 2004). Fig. 9a shows the effect of varying drain spacing on average drawdown on the sliding surface at the base of the aquifer at the steady state condition for different slope angles ( $\beta$ ) of  $10^{\circ}$ ,  $20^{\circ}$ ,  $30^{\circ}$  and

 $40^{\circ}$ , and aquifer/landslide length of  $L_{yD}=2.5$  and  $L_{yD}=5$ . Drain length was  $L_{dD}=2$ . Fig. 9a shows that by increasing the spacing between the drains the average drawdown of water head on the sliding surface at the base of the aquifer decreases. This inverse relationship between steady-state drawdown and drain spacing becomes amplified as slope angle increases from  $10^{\circ}$  to  $40^{\circ}$ . By increasing the drain spacing from 0.1 to 1.0, for slope angle of  $10^{\circ}$  and aquifer length of 2.5, the average normalized drawdown decreases from 0.18 to 0.15, whereas for a slope angle of  $30^{\circ}$ , the average drawdown decreases from 0.59 to 0.44, indicating the importance of dense drain arrays in steep aquifers. Even though steady state drawdown tends to increase with slope angle, the average drawdown of  $\beta=30^{\circ}$  is larger than that at  $\beta=40^{\circ}$ . This owes to aquifer geometry and slope angle on drain length, where increasing the slope angle from  $30^{\circ}$  to  $40^{\circ}$  restricts the capacity of drain to function beyond the depth of the aquifer.

Fig. 9b presents the absolute changes of mobilized friction angle at steady state conditions varying with drain spacing for different slope angles and aquifer lengths. As the drain spacing increases, the effectiveness of horizontal drains in improving the mobilized friction angle declines, due to sustained elevated head (i.e. higher pore water pressure) at steady state conditions. This also reflects the three-dimensional sensitivity of slope stability to localized drawdown conditions between drains. Following the same behavior as drawdown, the rate of mobilized friction angle improvement is expedited with increasing slope angle. For instance, by widening the drain spacing from 0.1 to 1.0 and  $L_{yD}=2.5$  for  $\beta=10^\circ$  and  $\beta=30^\circ$  the decline in mobilized friction angle improvement is 21 % and 23 %, respectively.

Fig. 9c shows the variation of total outflow discharge of the drain

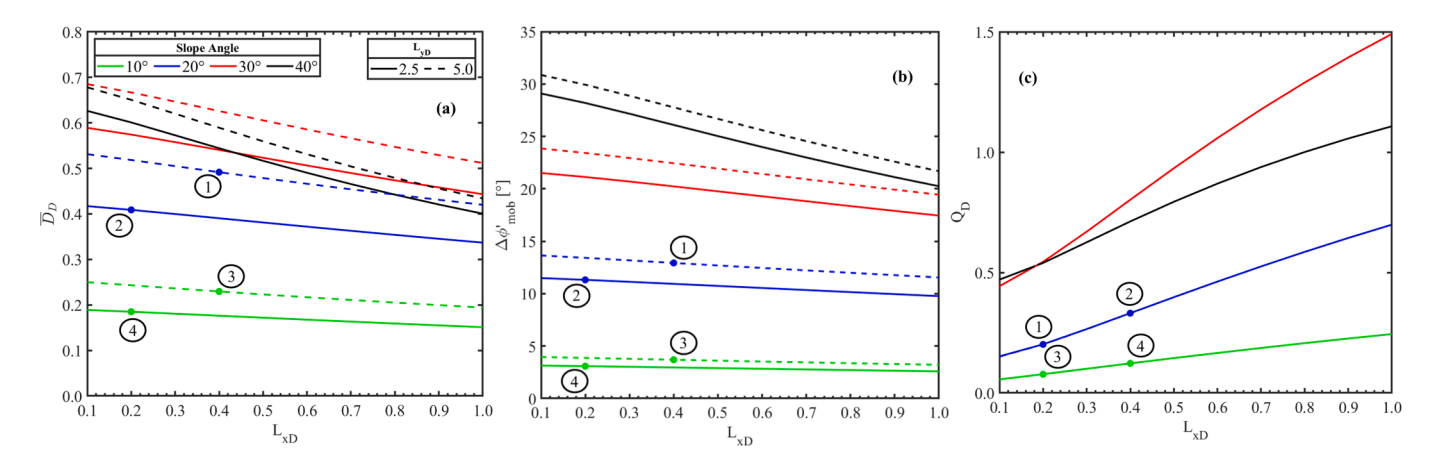


**Fig. 9.** Steady state (a) average drawdown, (b) mobilized friction angle at the slip surface corresponding to drawdown, (c) total outflow discharge of the drain vs drain spacing ( $L_{xD}$ ) for different slope angle (β) and aquifer length ( $L_{yD}$ ).

with drain spacing for different slope angles and aquifer lengths. As the total discharge is only dependent on length of the drain, unit cylindrical surface area surrounding the drain and hydraulic gradient in the vicinity of the drain. Therefore, the steady state condition total discharge of the drain is not sensitive to increasing aquifer lengths for the conditions presented (both lengths overlapped in Fig. 9c). Increasing the spacing between drains creates larger total steady-state outflow discharges, however, and discharge also increases with aquifer slope. The increasing total discharge with wider drain spacing indicates the significant effect of steady-state hydraulic gradient, which is higher in wider drain spacing due to higher steady state head (i.e. smaller drawdown) between drains spaced apart at significant distances.

Four distinct cases of drain and aquifer geometry specifications are chosen to show the time series for average drawdown and, changes in mobilized friction angle and total discharge. The four cases are marked on Fig. 10 with Case 1 and 2 representing a drain with a 20° slope angle and aquifer length of 5 and 2.5 and drain spacing of 0.4 and 0.2, respectively. Case 3 and 4 also represent aquifer length of 5 and 2.5 and drain spacing of 0.4 and 0.2, respectively, with drain in slope with 10° inclination. Fig. 10a shows the transient average drawdown for Cases 1 to 4. Comparing Cases 1 and 3 representing same aquifer length ( $L_{vD} =$ 5) and drain spacing ( $L_{xD} = 0.4$ ) reveals that installing the drain in steeper slopes results in larger volumes of water being removed which occurs in three distinct stages, however, the time it requires to achieve steady state conditions are similar were major water being drawn from aquifer at the third stage of drawdown (water extraction from upslope boundary). Comparing Cases 2 and 4 regarding same aquifer length  $(L_{yD}=2.5)$  and drain spacing  $(L_{xD}=0.2)$  also shows the three distinct stages of drawdown, where major groundwater drawdown has occurred at the initial stages and the average drawdown at the third stage is comparably smaller than first stage indicating smaller volume of water being drawn from the upslope.

Fig. 10b shows the transient absolute changes of mobilized friction angle corresponding to the average drawdown shown in Fig. 10a for Cases 1, 2, 3 and 4. Due to direct relationship between pore water pressure and enhancement of slope stability, changes in mobilized friction angle follows the same behavior as average drawdown. For Cases 2 and 4 which represent shorter drain spacing and aquifer length  $(L_{xD}=0.2 \text{ and } L_{yD}=2.5)$  the three stages of drawdown are noticeably visible and major changes of mobilized friction angle occurs at the first stage of drawdown which impact mostly surrounding of the drain. Cases 1 and 3 that are representative of longer drain spacing and aquifer length  $(L_{xD}=0.4 \text{ and } L_{yD}=5)$  show less gain in stability during the first and second stages of drawdown compared to Cases 2 and 4, respectively. However, by achieving steady state conditions, the stability gains for Cases 1 and 3 surpasses Cases 2 and 4, respectively.

Fig. 10c shows the transient total outflow discharge of the drains of

Cases 1, 2, 3 and 4. Cases 1 and 2 corresponding to HD installed in 20° slope angle shows significantly higher initial discharge rates comparing to Cases 3 and 4 (HD in 10° slope angle). Because the drain length is constant for all the cases, this is a result of higher initial hydraulic gradients in proximity of the drain for a 20° slope angle. In spite of the higher discharge rate at initial stages of drawdown, at the steady state condition all four cases have similar discharge rates (less than 0.4) indicating the primary control of drain length on discharge at steady state stage. Also, the length of the aquifer and/or drain spacing do not have significant effect on total discharge rate for Cases 3 and 4 which represent different drain spacing and aquifer lengths for slope angle of 10°. This can be explained by minor average drawdown (i.e. head) difference between Cases 3 and 4 (Fig. 10c). However, by increasing the slope angle to 20° (Cases 1 and 2), the effect of aquifer length becomes more notable specially at earlier stages of drawdown due to larger hydraulic gradients with wider drain spacing.

#### 5.4. Predictive model of drawdown

As the proposed numerical solutions can be computationally expensive, having a predictive model that predicts drawdown for simple site conditions is of value, at least as a low-cost, simple means of predicting drawdown. Thus, we develop a regression and tools based on Artificial Neural Networks (ANN) to predict transient drawdown from horizontal drains given any drain and aquifer conditions. The tool is thereafter implemented into an ArcGIS toolbox for easy application towards planning and scenarios, provided as supplementary information with this study. Artificial neural network (ANN) is a supervised machine learning algorithm and is used for classification of drawdown modeled by proposed numerical method in this study. For this purpose, the Rectified Linear Unit (ReLU) was chosen as the activation function and considering the regression nature of the problem the gradient decent function was chosen as back-propagation algorithm. The input layer of ANN consists of 5 neurons, representing the input features ( $L_{xD}$ ,  $L_{yD}$ ,  $L_{zD}$ ,  $L_{dD}$ , and  $\beta$ ), and the output layer has 1 neuron, yielding the drawdown. The number of hidden layer neurons was tested from 4 to 15 and the ANN model of 5-5-1 appeared to predict the transient drawdown behavior with the lowest mean squared error of 0.0015 for training and 0.0016 for testing.

Fig. 11a compares average groundwater drawdown on failure surface based on numerical model proposed in this study to the predicted values obtain by ANN model for different aquifer and drain condition selected for random times at transient state. The prediction accuracy of the ANN model is assessed by displaying 10 % and 25 % prediction lines. The average drawdown was estimated with RMSE of 0.037 and correlation coefficient of 0.98 which indicates high accuracy of the ANN model in predicting the drawdown for any condition. Fig. 11.b shows the

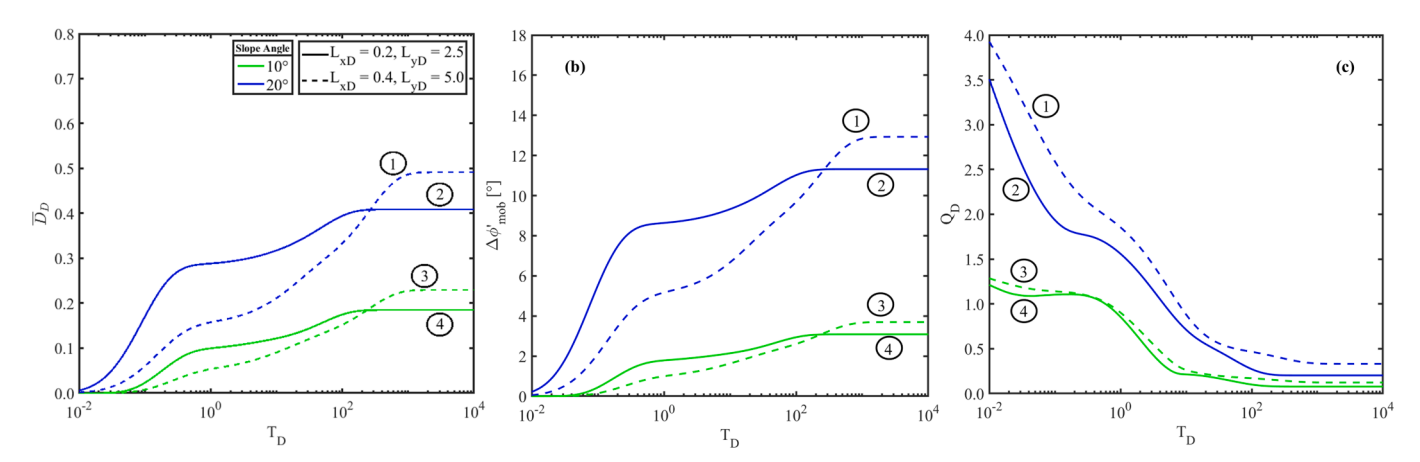


Fig. 10. (a) Transient average drawdown, (b) corresponding mobilized friction angle, (c) total outflow discharge for cases 1, 2, 3 and 4.

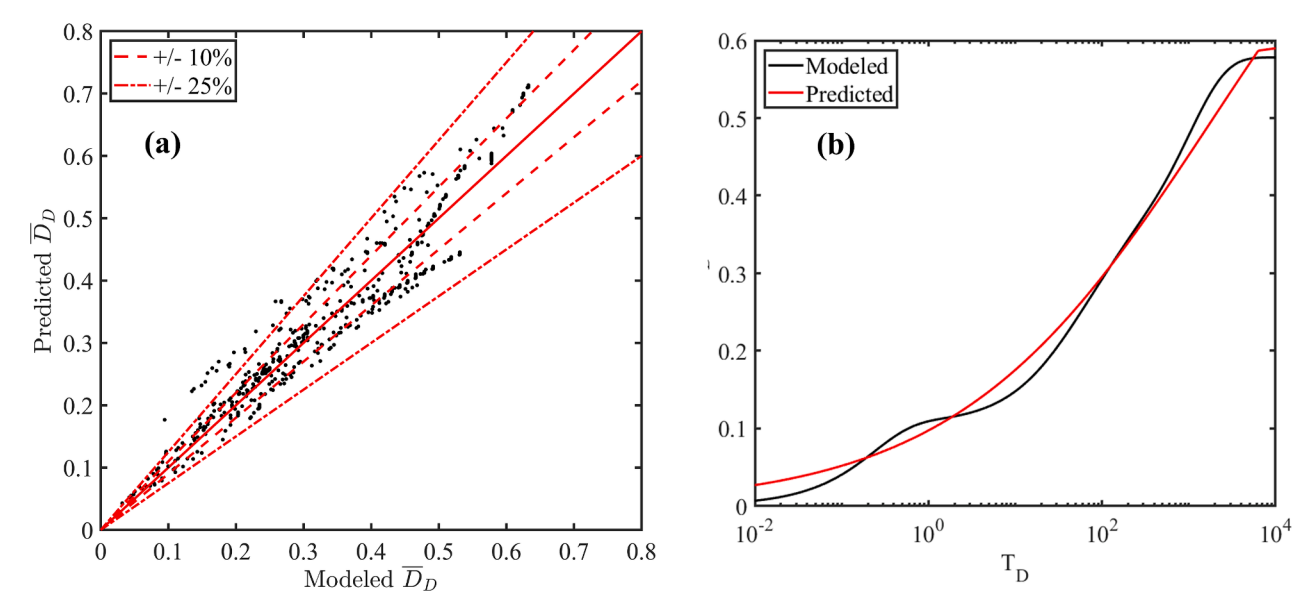


Fig. 11. (a) Scatter plot of modeled vs. predicted transient groundwater drawdown for different drain and aquifer specifications selected at random times; (b) Comparison of modeled and regression predicted transient groundwater drawdown for  $L_{dD} = 5$ ,  $L_{xD} = 1.6$ ,  $L_{yD} = 10$  and  $\beta = 10^{\circ}$ .

comparison of numerical modeling transient groundwater drawdown and regression predicted drawdown by ANN for  $L_{dD}=5$ ,  $L_{xD}=1.6$ ,  $L_{yD}=10$  and  $\beta=10^{\circ}$ . For these conditions, the RMSE is 0.017 and  $R^2$  of 0.99 indicating that ANN was capable of capturing the very nonlinear transient drawdown with minimal overestimation at early stage of drawdown. These regressions enable simplified application of planning-level drawdown predictions with the provided tools. Of course, more complex models could provide more accurate predictions based on the training data; future work could better parameterize transient drawdown predictions using more robust field data and modeling approaches.

## 6. Conclusions

Horizontal drains have proven to have significant effect on lowering the groundwater level and stabilizing slopes driven to instability from elevated groundwater levels. In this study a finite difference numerical solution for transient three-dimensional groundwater flow by gravity driven horizontal drains in an unconfined aquifer with an upslope recharge boundary condition was proposed. We validated the proposed method with semi-analytical solution proposed by Zhan and Zlotnik (2002) by changing the boundary conditions and modeling the drain with a pumping rate, showing good agreement with a semi analytical solution. We also compare our solution with physical model experimental study by Lakruwan et al. (2021) for two different constant head values, reasonable agreement is achieved when comparing steady-state drawdown conditions.

The three-dimensional transient solution was achieved through finite difference numerical method by modeling the drain as a constant elevation head boundary at the specific locations. The head at each time step was used to calculate pore water pressures and the corresponding slope stability, as well as discharge from the drain. We proposed the inputs and results in dimensionless form incorporating aquifer depth and soil and aquifer propeties to provide type curves for specific solutions and generalize the solution for any soil properties. Due to spatial variation of drawdown, the results were presented in terms of average drawdown on the slip surface. As a baseline condition, a specific drain and aquifer geometry was chosen to reflect three stages of transient groundwater drawdown, including (1) an initial rapid drawdown stage that reflects the formation of cone of depression in proximity to the drain, (2) an intermediate drawdown stage during which cone of

depression grows laterally and upslope and overall drawdown is slowed, and a (3) final drawdown stage where full cone of depression formation occurs laterally and upslope of the drain. Thereafter, steady state conditions are achieved. These mechanisms of drawdown vary with drain spacing, length, aquifer slope and boundary conditions. However, the drawdown is the most rapid and strong near the drain and is more diffuse with distance from the drain system, demonstrating that the three-dimensional considerations of this problem are likely non-trivial. Consequently, the magnitude and the rate of drawdown increases with decreasing drain spacing, increasing length and increasing aquifer slope as these conditions reduce the distance required to flow to a drain and increase hydraulic gradients, respectively. As expected, increasing drawdown increases stability (i.e. decreases mobilized friction for equilibrium).

A sensitivity analysis was performed to investigate the effect of varying drain length and drain spacing on average drawdown as these factors are primary design parameters. In the parametric studies, changes of mobilized friction angle and total outflow discharge were evaluated for different slope angles and aquifer lengths. For select cases, transient time series showing average drawdown, changes in mobilized friction angle and total outflow are shown. Stability, as expected, increases with drawdown. However, overall discharge decreases with drawdown as lowered head conditions decrease the hydraulic gradient and consequently flow rates. This analysis indicates the important role of drain length and spacing on controlling the drawdown. Further, it demonstrates that horizontal drains can be particularly effective from dewatering steeper aquifers. It was shown that drawdown and consequently mobilized friction angle is more sensitive to drain length. Steady state outflow discharge is primarily dependent on drain length and hydraulic gradient proximal to the drain systems. Increasing spacing between drains results in less drawdown owing to distinct threedimensional groundwater conditions - in some instances, ignoring these three-dimensional conditions may be unconservative. The proposed pore pressure fields are used to evaluate mobilized friction for a simple sliding plane; however, future work could (1) export the posed pore pressure fields for simple or complex stability analyses (e.g. optimization of slip surfaces and factor of safety using slope stability software), (2) use the simplified mean drawdown as an input for commercial slope stability (e.g. an average pore pressure or pore pressure ratio), and/or adapt the use of the numerical solution within slope stability software packages (e.g. commercial software).

A regression based on artificial neural network (ANN) was proposed to predict groundwater drawdown for aquifer and drain specifications and is implemented in a simple toolbox. The proposed regression was tested against the results of numerical solution proposed and demonstrated reasonable agreement for multiple aquifer and drain geometries. Such a tool enables users to determine simple estimates of drawdown for given site conditions without the need to perform numerical analyses. Future work could use more sophisticated models for training and analyzing drawdown data from models and the field; however, the proposed tools based on the numerical models posed herein may be of value for low-cost planning purposes.

#### CRediT authorship contribution statement

**Mahrooz Abed:** Data curation, Formal analysis, Investigation, Methodology, Supervision, Validation, Visualization, Writing – original draft, Writing – review & editing. **Bipin Peethambaran:** Funding acquisition. **Ben Leshchinsky:** Funding acquisition.

#### Declaration of competing interest

The authors declare that they have no known competing financial interests or personal relationships that could have appeared to influence the work reported in this paper.

#### Data availability

Data will be made available on request.

#### Acknowledgments

The authors gratefully acknowledge support from Oregon Department of Transportation grant SPR834. The second author also acknowledges support from NSF CMMI-2050047 and McIntire-Stennis project OREZ-FERM-898. Further, we appreciate the valuable comments provided by an editor and two anonymous reviewers.

## Appendix A. Supplementary data

Supplementary data to this article can be found online at https://doi. org/10.1016/j.compgeo.2023.106044.

#### References

Alberti, S., Leshchinsky, B., Roering, J., Perkins, J., Olsen, M.J., 2022. Inversions of landslide strength as a proxy for subsurface weathering. Nat. Commun. 13 (1), 6049.

- Cai, F., Ugai, K., Wakai, A., Li, Q., 1998. Effects of horizontal drains on slope stability under rainfall by three-dimensional finite element analysis. Comput. Geotech. 23 (4) 255–275
- Cornforth Consultants Inc "HORIZONTAL DRAINS 2012–2013 CONSTRUCTION SUMMARY REPORT Grading & Drainage." Geotechnical design report 2013 Oregon DOT Salem, OR.
- Crenshaw, B.A., Santi, P.M., 2004. Water table profiles in the vicinity of horizontal drains. Environ. Eng. Geosci. 10 (3), 191–201.
- Daviau, F., Mouronval, G., Bourdarot, G., Curutchet, P., 1988. Pressure analysis for horizontal wells. SPE Form. Eval. 3 (04), 716–724.
- Goode, P., Thambynayagam, R., 1987. Pressure drawdown and buildup analysis of horizontal wells in anisotropic media. SPE Form. Eval. 2 (04), 683–697.
- Hammond, C.M., Meier, D., Beckstrand, D., 2009. Paleo-landslides in the tyee formation and highway construction, central oregon coast range. Geol. Soc. Am. Field Guide 15, 481–494.
- Hooghoudt, S., 1940. General consideration of the problem of field drainage by parallel drains, ditches, watercourses, and channels. Contribution to the knowledge of some physical parameters of the soil 7.
- Hu, J., Ke, H., Zhan, L.T., Chen, Z.Y., Lan, J.W., Powrie, W., Chen, Y.M., 2020. Installation and performance of horizontal wells for dewatering at municipal solid waste landfills in China. Waste Manag 103, 159–168.
- Hu, J., Ke, H., Chen, Y.M., Xu, X.B., Xu, H., 2021. Analytical analysis of the leachate flow to a horizontal well in dual-porosity media. Comput. Geotech. 134.
- Huang, C.-S., Chen, Y.-L., Yeh, H.-D., 2011. A general analytical solution for flow to a single horizontal well by Fourier and Laplace transforms. Adv. Water Resour. 34 (5), 640–648.
- Hungr, O., Salgado, F.M., Byrne, P., 1989. Evaluation of a three-dimensional method of slope stability analysis. Can. Geotech. J. 26 (4), 679–686.
- Jones, T., Cartwright, T., Abed, M., Tardif, M., Robinson, L., Wurst, P., Mohney, C., Glover-Cutter, K., Leshchinsky, B., 2023. Developing systems-level criteria for evaluating performance of horizontal drains toward landslide mitigation: Case study of the US20 pioneer mountain-eddyville realignment project. J. Geotech. Geoenviron, Eng. 149 (5).
- Lakruwan, M., Oikawa, H., Kamura, A., Kazama, M., 2021. Experimental evaluation of effect of perforation arrangement on performance of horizontal drains in landslide mitigation. Landslides 18 (11), 3707–3714.
- Mohamed, A., Rushton, K., 2006. Horizontal wells in shallow aquifers: Field experiment and numerical model. J. Hydrol. 329 (1–2), 98–109.
- Rahardjo, H., Hritzuk, K.J., Leong, E.C., Rezaur, R.B., 2003. Effectiveness of horizontal drains for slope stability. Eng. Geol. 69 (3–4), 295–308.
- Rahardjo, H., Santoso, V.A., Leong, E.C., Ng, Y.S., Hua, C.J., 2011. Performance of horizontal drains in residual soil slopes. Soils Found. 51 (3), 437–447.
- Sari, P.T.K., Mochtar, I.B., Chaiyaput, S., 2023. Effectiveness of horizontal sub-drain for slope stability on crack soil using numerical model. Geotech. Geol. Eng. 41 (8), 4821–4844.
- Sawyer, C.S., Lieuallen-Dulama, K.K., 1998. Productivity comparison of horizontal and vertical ground water remediation well scenarios. Groundwater 36 (1), 98–103.
- Sedghi, M.M., Samani, N., Sleep, B., 2009. Three-dimensional semi-analytical solution to groundwater flow in confined and unconfined wedge-shaped aquifers. Adv. Water Resour. 32 (6), 925–935.
- $M.R.\ Taha\ Effectiveness\ of\ horizontal\ drains\ in\ improving\ slope\ stability:\ A\ case\ study\ of\ landslide\ event\ in\ Putra\ Jaya\ Precinct\ 9\ 2011\ Malaysia.$
- Tang, L., Tang, X.W., Liu, W., 2011. A case study of effect of horizontal drains on rainfall-induced landslide. Adv. Mat. Res. 250, 1834–1837.
- Zhan, H., Zlotnik, V.A., 2002. Groundwater flow to a horizontal or slanted well in an unconfined aquifer. Water Resour. Res. 38 (7).
- Zhang, X., Wang, H., Gao, Z., Xiang, K., Zhai, Q., Satyanaga, A., Chua, Y.S., 2023. Evaluation of the performance of the horizontal drain in drainage of the infiltrated water from slope soil under rainfall conditions. Sustainability 15 (19), 14163.